



Firing properties of a stochastic PDE model of a rat sensory cortex layer 2/3 pyramidal cell

Nicolangelo Iannella ^{a,*}, Henry C. Tuckwell ^{a,b}, Shigeru Tanaka ^a

^a *Laboratory for Visual Neurocomputing, Brain Science Institute, RIKEN, 2-1 Hirosawa Wako-shi, Saitama 351-0198, Japan*

^b *Epidémiologie et Sciences de l'Information, INSERM U444, Université Paris 6, 27 rue Chaligny, 75012 Paris, France*

Received 17 December 2002; received in revised form 21 October 2003; accepted 31 October 2003

Abstract

We have developed a non-linear stochastic PDE (partial differential equation) model of a rat layer 2/3 somatosensory pyramidal neuron which approximates several of the dynamical properties of these cells. The model distinguishes telodendrites, a myelinated axon, initial segment, hillock, soma and a simplified dendritic tree. Distributions and properties of excitatory and inhibitory synapses were included, in accordance with recent anatomical and physiological findings. Using simulation methods, we aim to show that the spatial separation between regions of spatially distributed randomly activated excitatory and inhibitory synaptic inputs may be an important parameter which can influence neuronal firing properties. Due to the complexity of the problem, with respect to configurations of spatially and temporally activated excitatory and inhibitory synaptic inputs, we consider two simple configurations in which the spatial region of activated excitatory and inhibitory synaptic inputs overlap and when they are far from each. In the first, denoted configuration **A**, activated excitatory and inhibitory synapses were located close to the soma. In the second, denoted configuration **B**, active inhibitory synapses were close the soma, while active excitatory synapses were located on distal regions of the dendrite. For the first configuration, we find that increases in the mean rate of inhibition results in an increase in the width of the firing rate tuning curves, and that for particular mean input frequencies of excitation, increasing the mean input rate of inhibition does not always imply that the neuron fires at a slower rate. Furthermore, we observed for mean input frequencies of excitation between 15 and 60 (Hz), that increasing the mean rate of inhibition resulted in the linearization of the firing rate over this interval. For configuration **B**, no increase in width nor a linearization effect via inhibition was observed. These differences indicate that the distance between regions of active excitatory and inhibitory synapses may be an important factor to consider in determining how the interaction between excitation and inhibition contributes to neuronal firing.

© 2004 Elsevier Inc. All rights reserved.

* Corresponding author. Tel.: +81-48 462 1111x7152; fax: +81-48 467 9684.

E-mail addresses: nicolang@brain.riken.go.jp, angelo@postman.riken.go.jp (N. Iannella).

Keywords: Input–output properties; Simplified spatial model; Pyramidal cell; Stochastic PDE

1. Introduction

Experimental studies have established that the response of individual cortical neurons, subject to (natural or artificial) stimulation, is highly variable. Understanding how the apparent randomness of neuronal firing is compatible with the coding of information in the central nervous system is of great interest. A closely related problem, how the cortical neuron transforms (spatio-temporal patterns of synaptic) input to output (i.e. input–output relation), is a fundamental question which has not been fully answered. One of the main obstacles in answering this question is the high degree of anatomical complexity of cortical neurons coupled with the complexity in the dynamics, interaction and modulation of different channel types. Many studies have considered point models which have ignored the influence of anatomical features of the cell in response to given time sequences of synaptic inputs [1–3]. In comparison, fewer studies have considered the spatial extent of neurons since the work of Rall [4] on passive cable theory and the pioneering deterministic study of Dodge and Cooley [5] on motoneurons although some authors have begun to employ spatial models for cortical neurons [6]. Most studies, which have considered spatially extended neurons, have used deterministic current injection (typically at a single site) to demonstrate an (almost) linear relationship between input current and firing rate of the model cell, where input current is usually varied over a range of several nanoamperes [7], using software packages like Neuron, Genesis and XBNC. Recently, Tuckwell et al. [8] analysed a linear cable model neuron driven by synaptic Ornstein–Uhlenbeck processes – see also [9–11] for previous analytical investigations of white noise driven cables. It is useful to consider model neurons with spatial extent, and to include as much anatomical and physiological detail as necessary without making the model excessively complicated.

We have chosen a model whose dynamics are described by a system of non-linear stochastic partial differential equations, and which approximates several of the dynamical properties of actual rat layer 2/3 pyramidal cells. A previous study had a similar aim but only considered deterministic current injection, using the Neuron software package [6]. In the construction of our simplified model, each cylindrical component is required to preserve the length, total surface area and the electrical properties of each corresponding region of the cell [12]. These regions were selected based upon the types of ionic currents present, the distribution of synapses and the morphology. Our simplified model reproduces the correct forms of EPSPs and IPSPs including rise times, decay times and amplitudes. It also has correct whole cell input resistance and time constant of somatic membrane potential decay. The model includes telodendria, a myelinated axon, initial segment, hillock, soma and components of a simplified dendritic tree. Furthermore, appropriate densities of sodium and potassium channels are added throughout but we have so far neglected various calcium channels and other voltage dependent potassium channels. Finally, suitably spatial distribution of excitatory and inhibitory synapses, with densities and properties according to recent electrophysiological data were included.

For the simplified model of a rat layer 2/3 pyramidal cell developed here, a method to construct a simplified dendrite, based upon the conservation of length, total surface area and the mean axial

resistance of selected dendritic regions of the cell is similar to a previously proposed method [12], but avoids the need of a computationally expensive fitting procedure to find values for the internal resistivity. Conserving the mean axial resistance, by appropriately scaling the internal resistivity, ensures that voltage attenuation is consistent with experimental observations. Using this model, we investigate the firing properties for two different spatial configurations of randomly activated synapses. Although one could have considered many different spatio-temporal patterns of synaptic input, for the sake of simplicity and clarity only the simplest patterns were considered. The first configuration consisted of activated excitatory and inhibitory synapses close to the soma. The second consisted of activated excitatory synapses located on distal dendritic regions and inhibitory synapses close to the soma. For both configurations, a non-linear input–output relationship was found. Furthermore, differences in the resulting histograms of the time to evoke the first action potential for the two configurations were investigated.

2. The stochastic PDE model of a rat layer 2/3 pyramidal cell

We consider a continuous spatially extended model of a layer 2/3 pyramidal neuron which extends from $x = 0$ to $x = L$ with depolarization $V = V(x, t)$ (in millivolts) at the space point x and time point t . Time and distance have the units of seconds and centimeters, respectively. The model pyramidal cell has as components telodendria, a myelinated axon, initial segment, hillock, soma and a simplified dendritic tree.

Stimulating the cell are N_E excitatory and N_I inhibitory afferent fibres each contributing n_E excitatory and n_I inhibitory synaptic inputs at points $x_{j,l}^E$ and $x_{k,m}^I$, respectively, where $j = 1, \dots, N_E$, $l = 1, \dots, n_E$, $k = 1, \dots, N_I$ and $m = 1, \dots, n_I$. The activation times of these afferent inputs are assumed to be random. In this first study, we let them be the event times of Poisson processes $N_{E,j}$ and $N_{I,k}$, assumed in the first instance to be temporally homogeneous with rate parameters $\nu_{E,j}$ and $\nu_{I,k}$, respectively. We then have

$$\begin{aligned}
 C_m \frac{\partial V}{\partial t} = & \frac{1}{2\rho_i a(x) \sqrt{1 + a'(x)^2}} \frac{\partial}{\partial x} \left(a^2(x) \frac{\partial V}{\partial x} \right) + I_{\text{ion}}(x, t), \\
 & + \left[\sum_{j=1}^{N_E} \sum_{n_j=1}^{\infty} H(t - T_{j,n_j}^E) \sum_{l=1}^{n_E} \delta(x - x_{j,l}^E) g_{j,l}^E(x, t - T_{j,n_j}^E) \right] (V_E - V) \\
 & + \left[\sum_{k=1}^{N_I} \sum_{n_k=1}^{\infty} H(t - T_{k,n_k}^I) \sum_{m=1}^{n_I} \delta(x - x_{k,m}^I) g_{k,m}^I(x, t - T_{k,n_k}^I) \right] (V_I - V), \tag{1}
 \end{aligned}$$

$$\frac{\partial m}{\partial t} = \frac{m_{\infty}(V) - m}{\tau_m(V)},$$

$$\frac{\partial h}{\partial t} = \frac{h_{\infty}(V) - h}{\tau_h(V)},$$

$$\frac{\partial n}{\partial t} = \frac{n_{\infty}(V) - n}{\tau_n(V)},$$

where the summation over the indices j and k denotes the sum over excitatory and inhibitory afferent fibres, respectively. Similarly, the summation over indices l and m represents the sum over contributed synapses from excitatory afferent j and inhibitory afferent k , respectively. Here, $a(x)$ is the radius of the cylinder at x , C_m is the membrane capacitance per unit area and ρ_i is the internal resistivity. V_E and V_I are the reversal potentials for excitation and inhibition, assumed to be the same for all synapses of a given type. The j th local conductance change in synapse l due to excitation starting at time zero is

$$g_{j,l}^E(x,t) = W^E(x) \left(\exp \left\{ -\frac{t}{\tau_d^E} \right\} - \exp \left\{ -\frac{t}{\tau_o^E} \right\} \right),$$

where $W^E(x)$ is the synaptic efficacy, τ_o^E and τ_d^E are the rise and decay time constants. Similarly for the k th local conductance change due to inhibition. $H(\cdot)$ is the Heaviside unit step function, T_{j,n_j}^E is the time of the n_j th event in the j th excitatory Poisson process and T_{k,n_k}^I is the time of the n_k th event in the k th inhibitory Poisson process. $I_{\text{ion}}(x,t)$ is the sum of voltage gated sodium, potassium and leak current densities, given by

$$I_{\text{ion}} = \bar{g}_{\text{Na}}(x)m^3h(V_{\text{Na}} - V) + \bar{g}_{\text{K}}(x)n(V_{\text{K}} - V) + \bar{g}_l(x)(V_l - V),$$

where V_{Na} and V_{K} are the Nernst potentials for sodium and potassium, respectively, and the quantity V_l is the equilibrium voltage for the leak current. $\bar{g}_{\text{Na}}(x)$, $\bar{g}_{\text{K}}(x)$ and $\bar{g}_l(x)$ are the corresponding sodium, potassium and leakage conductances per unit area and $n = n(x,t)$, $m = m(x,t)$ and $h = h(x,t)$ are the potassium activation, sodium activation and sodium inactivation variables, respectively. The equations describing the dynamics of the neuron are thus similar to the Hodgkin–Huxley equations for a cylinder of varying diameter in conjunction with stochastic synaptic input terms.

The steady state variable for sodium activation $m_\infty(V)$ and its corresponding time constant $\tau_m(V)$, are given by

$$m_\infty(V) = \frac{\alpha_m(V)}{\alpha_m(V) + \beta_m(V)} \quad \tau_m(V) = \frac{1}{\alpha_m(V) + \beta_m(V)},$$

where α_m and β_m are the voltage dependent forward and backward reaction rates, respectively. These reaction rates are given by

$$\alpha_m(V) = \frac{A_m(V - V_{m,1/2})}{1 - e^{-(V - V_{m,1/2})/K_m}} \quad \beta_m(V) = \frac{-A_m(V - V_{m,1/2})}{1 - e^{(V - V_{m,1/2})/K_m}},$$

where K_m determines the slope of the activation curve, and A_m is a rate constant. Similar expressions apply for the potassium activation but the corresponding steady state variable $h_\infty(V)$ is given by

$$h_\infty(V) = \frac{1}{1 - e^{((V - V_{h,1/2})/K_h)}}.$$

3. Model parameters derived from anatomical and physiological data

The simplified model was chosen to represent a rat layer 2/3 pyramidal cell taken from the barrel cortex. The anatomy of a typical cell [13] is depicted in Fig. 1. It was estimated that the actual cell had an area between 13 000–17 000 μm^2 . The estimated length of the apical dendrite and proximal trunk was 400 μm . The lengths of the basal dendrites varied from 30–150 μm . The dendrites were divided into three regions; the first 100 μm which contains the majority of basal dendrites, most of the apical dendritic proximal trunk and some sections originating from lateral obliques; the next 100 μm included the remaining sections from the proximal trunk, basal dendrites and lateral obliques; the final region of 200 μm , is comprised of the remaining apical dendrites. These three identified regions were used to construct a simplified dendritic tree.

The geometry of the model layer 2/3 pyramidal cell is represented by a continuous cylinder of varying diameter. In order to avoid jumps in diameter, the various components were joined by rapidly changing sigmoid functions. The total membrane surface area of the model pyramidal cell is approximately 15 000 μm^2 and its length is $L = 766 \mu\text{m}$. The simplified myelinated axon is similar to that used in a previous study [6], being composed of a hillock and initial segment whose combined length is 24 μm . There are two nodes of length 1 μm and diameter 1 μm each and three internodes of 100 μm myelin of diameter 1.5 μm and an axon terminal (representing telodendria) of length 22 μm and diameter 1 μm . The diameter of the axon initial segment is 1 μm while that of the hillock tapers from 4 to 1 μm , in a distance of 10 μm . The soma has a length of 18 μm and diameter of 8 μm . The simplified dendritic tree is composed of three connected cylinders representing the proximal, middle and distal parts. The dimensions are as follows: the corresponding lengths are 100, 100 and 200 μm , and the diameters are 16, 12 and 8 μm , respectively. These model parameters are summarized in Table 1.

Recent studies have revealed some details of the electrophysiology and distribution of synaptic contacts on pyramidal cells in the rat somatosensory cortex [13–15]. It has been found that a single afferent fibre, originating from a presynaptic neuron, typically contributes several widely

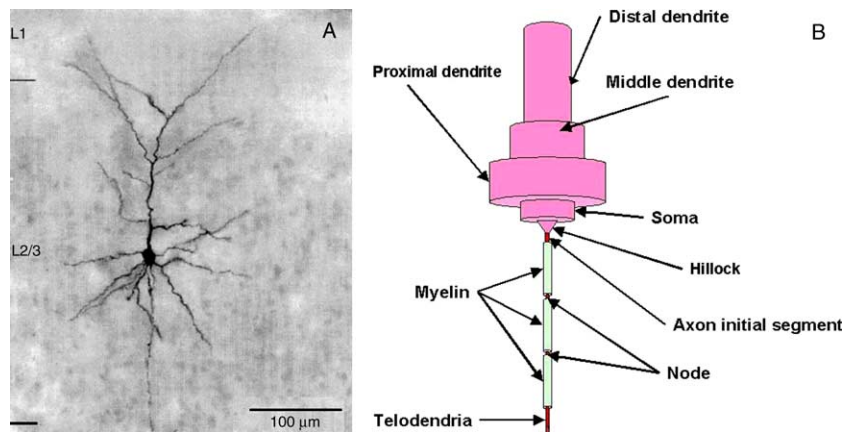


Fig. 1. (A) The anatomy of a typical layer 2/3 pyramidal neuron of the rat barrel cortex, adapted and modified from Feldmeyer et al. [13] with permission from both the authors and J. Physiology. (B) Approximating cylinder model.

Table 1
Dimensions of the model layer 2/3 pyramidal neuron

Component	Length (μm)	Diameter (μm)
Axon terminal	22	1
Myelin (3)	300	1.5
Nodes (2)	2	1
Initial segment	14	1
Hillock	10	Tapers from 4 to 1 μm
Soma	18	8
Proximal dendrite	100	16
Middle dendrite	100	12
Distal dendrite	200	8
Total length	766	

distributed synapses across the membrane of the pyramidal cell. The synapses originating from the afferents of presynaptic glutamatergic neurons evoke unitary excitatory post-synaptic potentials (uEPSPs), while those from the afferents of GABAergic neurons elicit unitary inhibitory post-synaptic potentials (uIPSPs) in the target pyramidal cell.

Both dual whole cell [14] and intracellular recordings [15] of the somatic membrane potential have revealed a variability in the size of unitary excitatory post-synaptic potentials (uEPSPs). Two separate studies, using dual somatic whole cell recordings, have demonstrated that there is a tendency for the average size of a unitary excitatory post-synaptic potential (uEPSP), as observed at the soma, to increase as the mean distance between soma and the synapses increases [13,14]. Ref. [14] showed that the average size of a uEPSP increases from 2 to 3 mV in a layer V pyramidal cell, as the mean distance of the synapses, from afferents originating in other layer V pyramidal cells, increases from soma to distal parts of the apical dendrite. A more recent study [13] found that the connections from layer 4 neurons to the basal dendrites of layer 2/3 pyramidal neurons are weak and that the mean size of the uEPSP increases from 0.4 mV at a distance of 40 μm to 0.7 mV at 120 μm from the soma. This study excluded connections originating from other pyramidal cells within layer 2/3, which form the major source of afferent inputs to a single layer 2/3 pyramidal cell, with synapses mainly on the apical dendrites. Apparently, no quantitative data is available for layer 2/3 cells on how the average size of somatically recorded uEPSPs varies as the mean distance between the synapses and the soma; hence data from layer V pyramidal cells was used. Furthermore, the first study suggest that a single afferent makes 5.5 synapses with the post-synaptic pyramidal cell [13], while the second reported an average of 4.5 synapses per afferent [13]. A value of 5 synapses per excitatory afferent fibre was therefore used in the model and the increase in uEPSP size with distance of source from soma was implemented by selecting various positions along the dendrite. At each selected position, while only activating 5 synapses, the synaptic efficacy was adjusted by trial and error until the size of the resultant EPSP observed in the soma of the model was similar to that observed from experiment [14]. The variation in synaptic strength along the dendrite is displayed in Fig. 2, was fitted by the following function $W_E(x)$, given by

$$W(x) = B * [9.5 / (1 + \exp(-(x - 200)/65)) + 0.85] \quad B = 2.3077 \times 10^{-4} \text{ (units of S/cm}^2\text{)}.$$

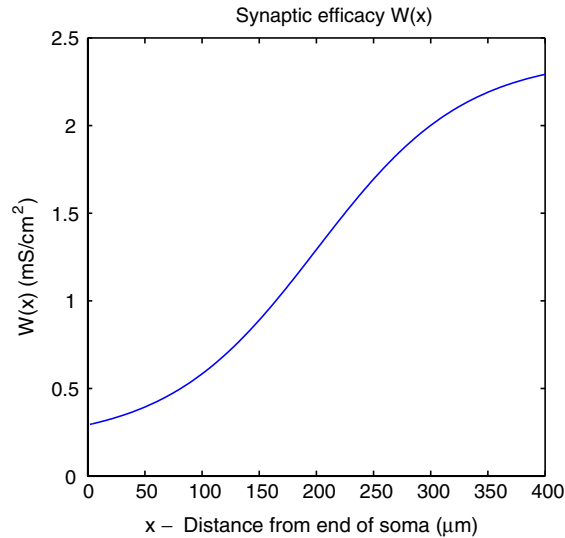


Fig. 2. The synaptic efficacy function $W(x)$ used to scale the size of the excitatory conductance, is displayed in units of mS/cm^2 .

The sizes of IPSPs are more uncertain. Some studies from rat neocortex suggest that a single activated GABAergic synapse located at the soma causes an approximate 2 mV hyperpolarization [16,17]. However, there is no information regarding how the average size of somatically recorded uIPSPs (and IPSPs) varies with the distance between the synapses and the pyramidal cell soma. Therefore, the following assumptions were made. Firstly, a single synapse, located at the soma, causes a 2 mV hyperpolarization when the cell is at rest. Secondly, each (GABAergic) afferent fibre was assumed to contribute 5 synapses and finally, the efficacy of single synapses was identical for all inhibitory synapses located on the soma, hillock and axon initial segment, with a value of $W_I(x) = 0.0623 \text{ S}/\text{cm}^2$. For the remaining synapses the efficacy was set to $W_I(x) = 0.00166 \text{ S}/\text{cm}^2$.

Excitatory and inhibitory synapses were distributed throughout the model neuron by initially assigning a unique centre to each excitatory and inhibitory input afferent, respectively and then randomly distributing its 5 synapses within an interval containing the centre at positions $x_{j,l}^E$ for excitatory and $x_{k,m}^I$ for inhibitory afferents, respectively.

Previous anatomical studies in rat [18] have estimated that the total numbers of glutamatergic and GABAergic synapses on an individual layer 2/3 pyramidal cell range from 3000 to 20 000 and 1000 to 3000, respectively. Furthermore, the following densities of synapses per $100 \mu\text{m}^2$ can be estimated from different morphological studies [18,19] as summarized in [20]: 55–65 glutamatergic synapses and 8–12 GABAergic throughout the dendritic tree, 40–80 GABAergic synapses in the axon initial segment and 10–20 GABAergic synapses in the soma. Using the mean of these synaptic densities led to estimates of a total of 8250 excitatory synapses originating from 1650 afferent fibres and 1475 inhibitory synapses from 295 afferents.

Recent studies indicate that the membrane capacitance per unit area ranges from 0.78 to 0.96 $\mu\text{F}/\text{cm}^2$ [21]; a value of 0.9 $\mu\text{F}/\text{cm}^2$ was adopted in the soma and dendrites. The internal resistivity

Table 2
Parameters describing Na⁺ and K⁺ channel kinetics

Channel	Variable	Function	A	$V_{1/2}$	K
Na ⁺	m	α_m	0.182	-35	9
		β_m	0.124	-35	9
	h	α_h	0.024	-50	5
		β_h	0.0091	-75	5
		h_∞	–	-65	6.2
K ⁺	n	α_n	0.02	20	9
		β_n	0.002	20	9

has an assumed value of 200 Ω cm [6]. The kinetic parameters of sodium and potassium channels, given in Table 2, were those used in [6], based on data from isolated rat neocortical pyramidal neurons.

The corresponding channel densities for the axon were identical to those of Mainen et al. [6] but channel densities in the dendrites were in accordance with previous observations [22,23]; $\bar{g}_{\text{Na}}(x) = 100$ pS/ μm^2 and $\bar{g}_{\text{K}}(x) = 80$ pS/ μm^2 . In order to reproduce attenuation as observed in experiments [12], the resistivity ρ_i of the proximal, middle and distal dendrite was scaled up by the ratio of cross sectional area of the model section and the mean cross sectional area in the corresponding region of the actual pyramidal cell. These led to the following values for the resistivity; $200 \times (8/0.825)^2 = 18806$ Ω cm for the proximal dendrite, $200 \times (6/0.75)^2 = 12800$ Ω cm for the middle dendrite and $200 \times (4/0.6)^2 = 8889$ Ω cm for the distal dendrite. The electrical properties are summarized in Table 3.

The system of equations (1) is solved numerically, using a modified Crank–Nicolson scheme to allow for non-linear terms [24,25] and sealed end boundary conditions [25]. We used $\Delta x = 2$ μm (384 space points) and a $\Delta t = 20$ μs . The times of events in homogeneous Poisson processes were generated using library generators of uniformly distributed random variables. The synaptic onset and decay time constants for excitation were set at $\tau_o^E = 0.2$ ms and $\tau_d^E = 1.5$ ms, respectively whereas, for inhibition, $\tau_o^I = 1.2$ ms and $\tau_d^I = 9$ ms. These onset and decay times were assumed to be the same for all synapses of a given type. For excitatory synapse, the onset and decay times were determined, so that a single EPSP located in the proximal dendrite would reproduce a similar profile as the EPSP in [13].

4. Results

Two simple spatial configurations of active afferent inputs, were chosen to investigate differences in input/output properties of the model pyramidal cell. For the first input pattern, the following configuration of active excitatory and inhibitory afferents are considered. Only the first 100 excitatory afferent input fibres (500 synapses), with centres close to the soma, and the initial 21 inhibitory afferents (105 synapses), with synapses proximal to the soma, were activated. The second input pattern consisted of changing the location of active excitatory synapses from

Table 3
Membrane parameters for model layer 2/3 pyramidal cell

Parameter	Symbol	Region	Value	Units
Resting potential	V_{rest}	Entire neuron	-70	mV
(Scaled) resistivity	ρ	Proximal dendrite	$200 \times (8/0.825)^2 = 18\,806$	$\Omega\text{ cm}$
		Middle dendrite	$200 \times (6/0.75)^2 = 12\,800$	$\Omega\text{ cm}$
		Distal dendrite	$200 \times (4/0.6)^2 = 8889$	$\Omega\text{ cm}$
		Elsewhere	200	$\Omega\text{ cm}$
Membrane capacitance/unit area	C_m	Myelin	0.04	$\mu\text{F}/\text{cm}^2$
		Elsewhere	0.9	$\mu\text{F}/\text{cm}^2$
Leak conductance/unit area	\bar{g}_l	Node	200	$\text{pS}/\mu\text{m}^2$
		Elsewhere	0.25	$\text{pS}/\mu\text{m}^2$
Na^+ conductance/unit area	\bar{g}_{Na}	Soma and dendrite	100	$\text{pS}/\mu\text{m}^2$
		Node	30\,000	$\text{pS}/\mu\text{m}^2$
		Myelin	30	$\text{pS}/\mu\text{m}^2$
K^+ conductance/unit area	\bar{g}_K	Soma & dendrite	80	$\text{pS}/\mu\text{m}^2$
		Elsewhere	0	$\text{pS}/\mu\text{m}^2$
<i>Reversal potentials</i>				
Leak	V_l	Entire neuron	-70	mV
Na^+	V_{Na}	''	30	mV
K^+	V_K	''	-90	mV
Excitation	V_E	''	-10	mV
Inhibition	V_I	''	-80	mV

Note: ‘Node’ indicates the initial segment, axon hillock, nodal membrane and axon terminal.

positions near the soma to distal regions of the dendrite. The positions of active inhibitory synapses were not changed. We will denote these spatial arrangements of active fibres as configurations **A** and **B**, respectively.

For both configurations **A** and **B**, the mean firing rate, mean interspike interval (ISI), the coefficient of variation (CV) and standard deviation are shown as a function of the mean input frequency in these excitatory afferents are shown in Figs. 3(A)–(D) and 5(A)–(D) respectively. These are given without inhibition and with inhibition at various indicated frequencies. For each combination of mean excitatory and inhibitory frequencies in Figs. 3 and 5, a total of 80 action potentials were gathered. Action potentials were counted by recording the time at which the membrane potential, in the second node (from the initial segment), crossed a threshold of -40 mV provided that the slope was positive. The mean firing rate was defined as the inverse of the mean interspike interval. This measure was also compared to the classical definition, i.e. the ratio between the number of spikes to be collected in one trial and the total time taken (time averaged firing rate); again difference was negligible.

The mean time to first spike and the corresponding standard deviation are also given as a function of mean input frequency of excitatory afferents, for each configuration **A** and **B** as shown in Figs. 4 and 6, respectively. These are also given with and without inhibition at various indicated frequencies. This time was measured as the time taken to evoke the first action potential from time

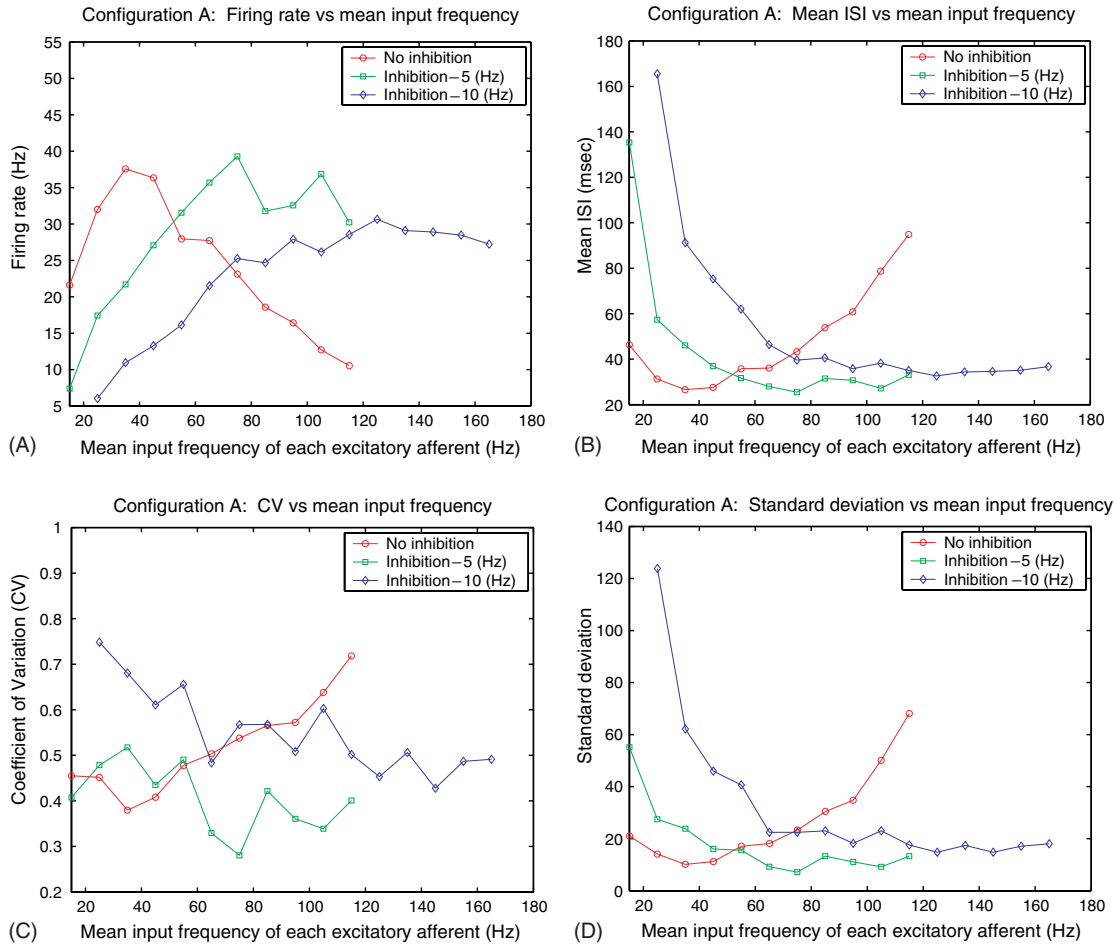


Fig. 3. (A) Plots of the mean firing rate as a function of mean input frequency of the first 100 excitatory afferent fibres, subject to different levels of inhibition. Active inhibitory afferents were activated at mean input frequencies of 2.5, 5 and 10 (Hz). The case when no inhibitory afferents were active, is also shown. The corresponding curves for the mean ISI, coefficient of variation and standard deviation of the ISI are shown in (B)–(D), respectively.

zero. A total of 40 trials were used to calculate the mean time to first spike and the corresponding standard deviation for the various combinations of mean input frequencies in active excitatory and inhibitory afferent fibres.

For configuration A, it can be seen in Fig. 3(A), that the relationship between firing rate and the mean excitatory input frequency is not linear. Additionally, there is a tendency for the width of the resulting firing rate tuning curves to increase as the mean frequency of inhibition increases. This tendency is also evident in Fig. 3(B)–(D). By reference to Fig. 3(A), it can be seen that a greater frequency of inhibition does not always imply that the neuron is firing more slowly. Moreover, it can also be observed that the slope of the firing rate curve over the initial rising phase decreases as a function of mean input frequency of each inhibitory afferent. From the firing rate curves over the interval from 15 to 60 (Hz) of mean input frequency in each excitatory afferent, it

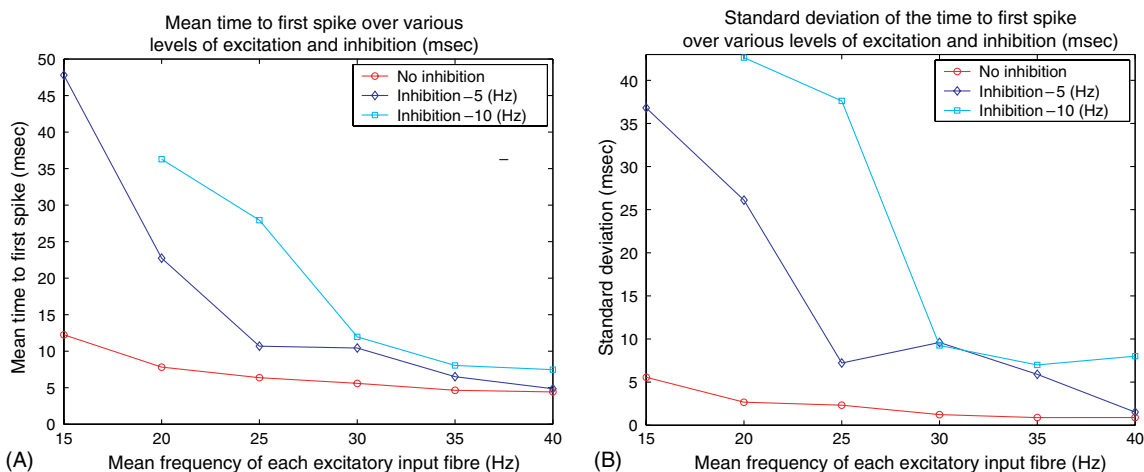


Fig. 4. (A) The mean time to first spike, resulting from the activation of 100 excitatory and 21 inhibitory afferent fibres, whose synapses are close to the soma. (B) The standard deviation of the time to first spike.

can be clearly observed that increasing the mean input frequency of inhibitory afferents results in the linearization of the firing rate. This effect is comparable to a previous simulation study [1] which illustrated a similar linearization effect using the Hodgkin–Huxley model driven by a constant input current with Gaussian white-noise of increasing variance.

The mean time to first spike and the corresponding standard deviation as a function of mean input frequency of excitation, subject to no inhibition and inhibition activated at the mean input frequencies of 5 and 10 Hz, is presented in Fig. 4. In Fig. 4(A) and (B), it is evident that at any given mean input frequency of excitation, the mean time to evoke an action potential and the standard deviation increases as the mean frequency of the active inhibitory afferents is raised. However, from Fig. 4(B), we see from the standard deviation for the respective mean input frequencies of 5 and 10 Hz on each inhibitory afferent, that a higher mean input frequency of excitatory afferents does not always imply less variability in the time to evoke the initial action potential.

We now present results for configuration **B** to see the effects of changing the location of active excitatory synapses to the distal region of the dendrite. In Fig. 5(A)–(D), we show the mean firing rate, mean ISI, CV and standard deviation, while in Fig. 6(A)–(B) the mean time to first spike and corresponding standard deviation are presented. For configuration **B**, it can be seen in Fig. 5(A) that the relationship between the firing rate and input frequency is non-linear, but the increase in width of these tuning curves and the associated ‘linearization effect’ was not evident. This effect is due to the distance between excitatory and inhibitory inputs. In configuration **A**, the regions where excitatory and inhibitory synaptic inputs are active overlap, unlike those of configuration **B**, whose corresponding regions are not overlapping. For configuration **A**, these overlapping regions of active excitatory and inhibitory synapses allow EPSPs and IPSPs to interact and summate. For configuration **B**, Fig. 5(A) indicates that the interaction between excitation and inhibition is quasi-linear, since, for a given level of inhibition A , the firing rate is approximately equal to the sum of the firing rate when no inhibition is present minus a constant. This form of

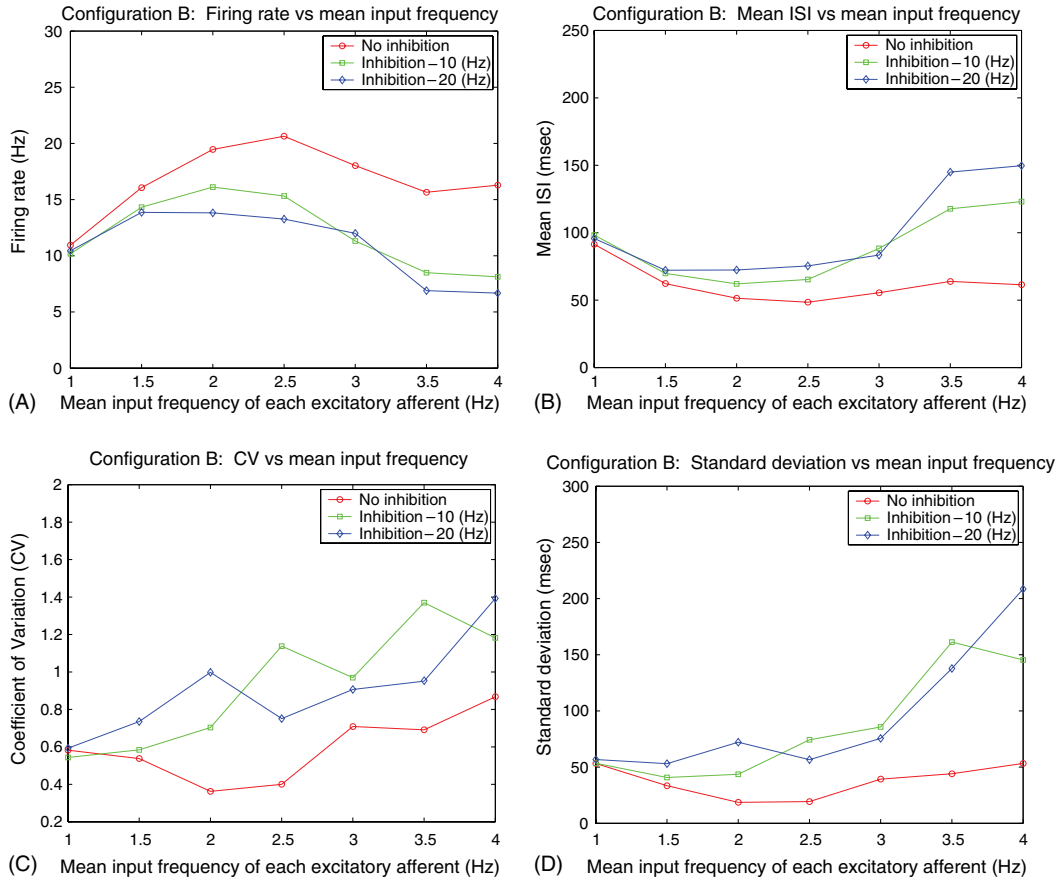


Fig. 5. (A) Tuning curves of the mean firing rate as a function of mean input frequency for configuration **B**. Active inhibitory afferents were activated at mean input frequencies of 10 and 20 (Hz). The case when no inhibitory afferents were active, is also presented. The corresponding curves for the (B) mean ISI, (C) coefficient of variation and (D) standard deviation of the ISI.

linearity in the firing rate should correlate with the summation of subthreshold synaptic inputs. Furthermore, passive cable theory indicates that for configuration **B** the summation of an EPSP and a IPSP is nearly linear in the soma, whereas for **A**, summation is not linear.

The mean time to first spike and the corresponding standard deviation for configuration **B** are shown in Fig. 6. Here, we also find a similar effect as observed for configuration **A** that at higher mean input frequency of excitatory afferents does not always imply less variability in the time to evoke the initial action potential.

In Fig. 7, we show what happens to the distribution of times to evoke the first spike when changing from configuration **A** to **B**. For both cases, the mean input frequency on each excitatory afferent is 20 Hz while the mean frequency of the (21 active) inhibitory afferents is 10 (Hz). The resulting distributions of the time to first spike are shown in Fig. 7. The mean time to first spike for configuration **A** was 22.66 ms, whereas for configuration **B**, the mean time was 8.29 ms.

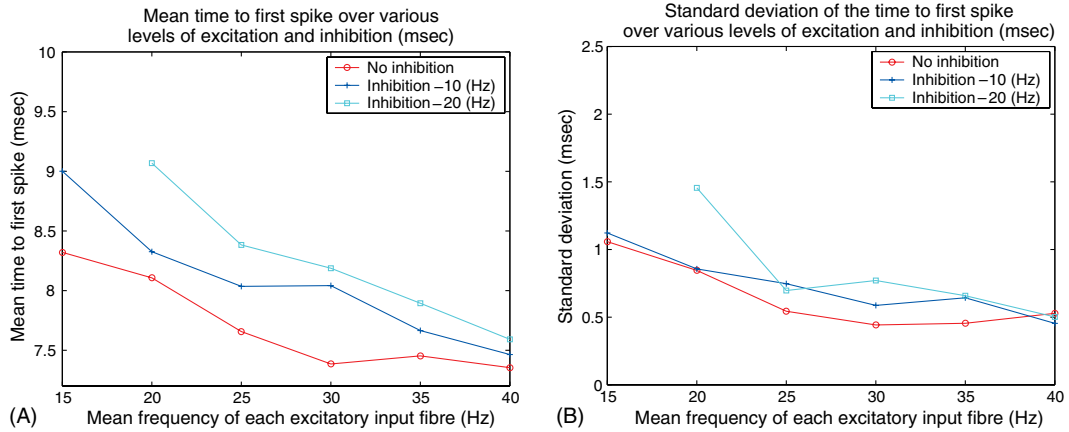


Fig. 6. (A) The resulting mean time to first spike for configuration **B**, whose synapses are close to the soma. (B) The corresponding standard deviation of the time to first spike.

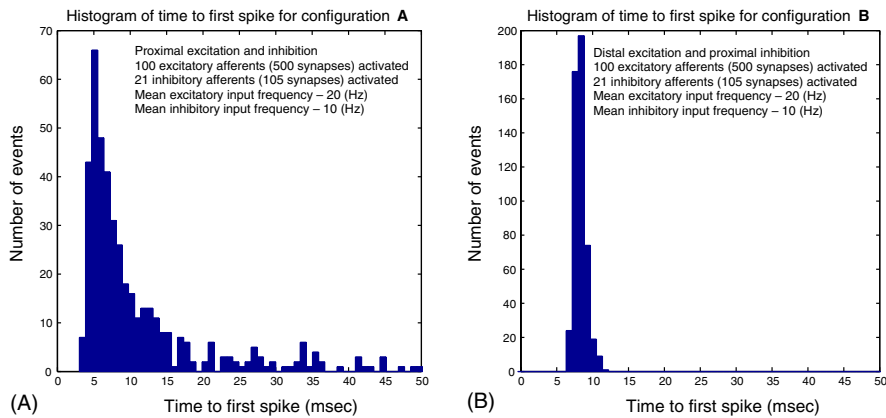


Fig. 7. (A) The histogram of time to first spike for configuration **A** excitatory afferents at a mean frequency of 20 (Hz), while the mean input frequency in inhibitory afferents was 10 (Hz). (B) The corresponding histogram of the time to first spike for configuration **B**, inhibitory and excitatory afferents were activated at mean input frequency of 10 and 20 (Hz), respectively.

Furthermore, Fig. 7 shows that for inhibitory synapses near the soma, there is much greater variability in the time to evoke the first spike when excitatory synapses are located near the soma rather than on the distal dendrites.

5. Conclusions

We have developed a simplified model of a rat layer 2/3 pyramidal cell, based upon a very simple construction method which conserves the electrical properties, length and total surface area

of selected regions of the original cell. In building our simplified model, we included relevant anatomical and physiological data with respect to the rat somatosensory system. If data was lacking for somatosensory layer 2/3 pyramidal cells, then data from layer 5 pyramidal neurons was used. In this initial study, we have not included the different types of calcium channels and various other potassium channels (like the high voltage activated calcium channel and the A-current) which are present in real cells. The effects that these other channels will have on the firing properties may be presented in the future.

We used this model to firstly demonstrate novel firing properties and secondly to show what happens when different spatial configurations of activated afferents inputs are used to stimulate a neuron. We considered two simple but different spatial configurations of afferent inputs, called **A** and **B**. For both configurations, we found that when the mean input frequency of excitatory inputs is increased, the firing rate initially increases, levels off and then decreases for high values. We also found that for configuration **A**, the width of the firing rate tuning curves increases as the mean input frequency in each active inhibitory afferent increased. This indicated that increasing the mean input rate of inhibition increases the range of mean excitatory input frequencies so that the cell can respond to higher mean frequencies in activated excitatory afferents. Furthermore, it was observed that over a finite interval of mean input frequencies of excitatory afferents (between 15 and 60 (Hz)), the firing rate was linearized as the mean frequency of inhibition was increased. When configuration **B** was used, as for configuration **A**, a non-linear relationship between the mean input frequency and firing rate was found but the observed ‘linearization effect’ and widening of these tuning curves was not present. This indicates that the spatial separation between excitatory and inhibitory inputs is the cause of differences between results for the two configurations.

It is pointed out that for configuration **A**, the increase in width of the firing rate tuning curves indicates that inhibition located close to the soma can directly modulate the total contribution of sodium currents to the generation of action potentials, consistent with previous studies [1,26]. Moreover, the linearization effect, associated with an increase of mean input frequency in inhibitory afferents, as observed in Fig. 3(A) over the range of frequencies between 15 and 60 (Hz) also indicates that inhibition may also modulate the firing rate when both excitatory and inhibitory synapses are located close to each other. Although it has been previously demonstrated that inhibition can increase the firing rate [27], this is clearly not always the case since this effect depends on the intrinsic properties of the membrane, the mean input frequency and the spatial separation of excitatory and inhibitory synapses. This effect occurs only when inhibition is close to excitation, which could not be predicted by a point model.

We point out that a non-linear relationship between firing rate and input has been indirectly observed for both in-vitro and in-vivo experiments [23,28] and can be simply accounted for by the inactivation of sodium channels, when the cell is sufficiently depolarized, in conjunction with an increase in outward potassium currents.

Additionally, the time to evoke the first action potential was calculated for both configurations while systematically varying the mean input frequencies of activated excitatory and inhibitory afferents. The resulting mean time to evoke the first action potential was compared for both configurations at a mean input frequency for excitation of 20 (Hz) and for inhibition 10 (Hz). With inhibition and excitation near the soma, the mean time to first spike was 22.66 ms whereas with the same inhibition but excitation on the remote part of the simplified dendritic tree the mean

was 8.29 ms. Furthermore, the distribution of times to evoke the first action potential differed considerably [11].

Although we have included many of the known data on the layer 2/3 pyramidal cells, several important data beg to be addressed experimentally. One example is whether the size of a single or unitary EPSP observed in the soma does increase as a function of distance from the soma. Current evidence is only provided for the basal dendrites, and its not unreasonable to expect a similar increase in somatic uEPSP size for synapses along the apical dendrite like that of layer V pyramidal cells [14]. Another question which needs to be addressed is whether IPSPs size also changes as a function of distance from the soma.

The differences in the distributions and the observed increase in width of the resulting firing rate curves for configuration **A** but not for configuration **B** suggests that the distance between regions of active excitatory and inhibitory synapses is an important factor in determining neuronal firing properties. Furthermore, these differences indicate that much further investigation with regard to the locations of activated synapses will be required to determine the possible error in point model approximations to real neurons. Conclusions from point models in relation to ‘configuration processing’ may be of dubious validity.

Acknowledgements

This work is supported by Riken, Brain Science Institute.

References

- [1] X. Lu, E.R. Lewis, Studies with spike initiators: linearization by noise allows continuous signal modulation in neural networks, *IEEE Trans Biomed. Eng.* 36 (1989) 36.
- [2] N. Brunel, P.E. Latham, Firing rate of the noisy quadratic integrate-and-fire neuron, *Neural Computat.* 15 (2003) 2281.
- [3] R.B. Stein, A theoretical analysis of neuronal variability, *Biophys. J.* 5 (1965) 173.
- [4] W. Rall, Theoretical significance of dendritic trees for neuronal input–output relations, in: R.F. Riess (Ed.), *Neural Theory and Modeling*, Stanford University, 1964, p. 73 (Chapter 4).
- [5] F.A. Dodge, J.W. Cooley, Action potential of the motoneuron, *IBM J. Res. Devel.* 17 (1973) 219.
- [6] Z.F. Mainen, J. Joerges, J.R. Huguenard, T.J. Sejnowski, A model of spike initiation in neocortical pyramidal cells, *Neuron* 15 (1995) 1427.
- [7] G.R. Holt, C. Koch, Shunting inhibition does not have a divisive effect on firing rates, *Neural Computat.* 9 (1997) 1001.
- [8] H.C. Tuckwell, F.Y.M. Wan, J.-P. Rospars, A spatial stochastic neuronal model with Ornstein–Uhlenbeck input current, *Biol. Cybernet.* 86 (2002) 137.
- [9] H.C. Tuckwell, J.B. Walsh, Random currents through nerve membranes i. uniform Poisson or white noise current in one dimensional cables, *Biol. Cybernet.* 49 (1983) 99.
- [10] H.C. Tuckwell, F.Y.M. Wan, The response of a nerve cylinder to spatially distributed white noise inputs, *J. Theor. Biol.* 87 (1980) 275.
- [11] H.C. Tuckwell, F.Y.M. Wan, Y.S. Wong, The interspike interval of a cable model neuron with white noise input, *Biol. Cybernet.* 49 (1984) 155.
- [12] A. Destexhe, Simplified models of neocortical pyramidal cells preserving somatodendritic voltage attenuation, *Neurocomputing* 38–40 (2001) 167.

- [13] D. Feldmeyer, J. Lubke, R.A. Silver, B. Sakmann, Synaptic connections between layer 4 spiny neurone-layer 2/3 pyramidal cell pairs in juvenile rat barrel cortex: physiology and anatomy of interlaminar signalling within a cortical column, *J. Physiol.* 538 (3) (2002) 803.
- [14] H. Markram, J. Lubke, M. Frotscher, A. Roth, B. Sakmann, Physiology and anatomy of synaptic connections between thick tufted pyramidal neurones in the developing rat neocortex, *J. Physiol.* 500 (2) (1997) 409.
- [15] A.M. Thomson, J. Deuchars, D.C. West, Relationships between morphology and physiology of pyramid–pyramid single axon connections in rat neocortex in vitro, *J. Physiol.* 478 (3) (1994) 423.
- [16] A.M. Thomson, A. Destexhe, Dual intracellular recordings and computational models of slow inhibitory postsynaptic potentials in rat neocortical and hippocampal slices, *Neuroscience* 92 (1999) 1193.
- [17] A.M. Thomson, D.C. West, Y. Wang, A.P. Bannister, Synaptic connections and small circuits involving excitatory and inhibitory neurons in layers 2–5 of adult rat and cat neocortex: triple intracellular recordings and biocytin labelling in vitro, *Cereb. Cort.* 12 (2002) 936.
- [18] A.L. Larkman, Dendritic morphology of pyramidal neurones of the visual cortex of the rat: iii. spine distributions, *J. Comparat. Neurol.* 306 (1991) 332.
- [19] J. DeFelipe, I. Farinas, The pyramidal neuron of the cerebral cortex: morphology and chemical characteristics of the synaptic input, *Prog. Neurobiol.* 39 (1992) 563.
- [20] D. Paré, E. Shink, H. Gaudreau, A. Destexhe, E.J. Lang, Impact of spontaneous synaptic activity on the resting properties of cat neocortical pyramidal neurons in vivo, *J. Neurophysiol.* 79 (1998) 1450.
- [21] A.J. Trevelyan, J.J.B. Jack, Detailed passive cable models of layer 2/3 pyramidal cells in rat visual cortex at different temperatures, *J. Physiol.* 539 (2) (2002) 623.
- [22] J.R. Huguenard, O.P. Hamill, D.A. Prince, Developmental changes in Na⁺ conductances in rat neocortical neurons: appearance of a slowly inactivating component, *J. Neurophysiol.* 59 (1988) 778.
- [23] O.P. Hamill, J.R. Huguenard, D.A. Prince, Patch-clamp studies of voltage-gated currents in identified neurons in the rat cerebral cortex, *Cereb. Cort.* 1 (1991) 48.
- [24] M.V. Mascagni, A.S. Sherman, *Methods in Neuronal modeling: From Ions to Networks*, 2nd Ed., MIT, 1999.
- [25] H.C. Tuckwell, Introduction to theoretical neurobiology, in: *Nonlinear and Stochastic Theories*, vol. 2, Cambridge University, New York, 1988.
- [26] D. Paré, E.J. Lang, A. Destexhe, Inhibitory control of somatodendritic interactions underlying action potentials in neocortical pyramidal neurons in vivo: an intracellular and computational study, *Neuroscience* 84 (1998) 377.
- [27] S. Feerick, J. Feng, D. Brown, Inhibitory inputs increase a neurons's firing rate, *Neurocomputing* 38–40 (2001) 197.
- [28] C. Monier, F. Chavane, P. Baudot, L.J. Graham, Y. Frégnac, Orientation and direction selectivity of synaptic inputs in visual cortical neurons: a diversity of combinations produces spike tuning, *Neuron* 37 (2003) 663.